Journal of Alloys and Compounds, 194 (1993) 417–427
JALCOM 7225

A molecular dynamics study of atomic level stress distributions in defective intermetallics*

D. T. Kulp, T. Egami, D. E. Luzzi and V. Vitek
Department of Materials Science and Engineering, University of Pennsylvania, Philadelphia, PA 19104 (USA)

(Received July 14, 1992; in final form September 15, 1992)

Abstract

A computer simulation study, using Finnis–Sinclair-type *N*-body potentials, of the amorphization of crystalline $CuTi_2$ by electron bombardment was carried out. It was shown that the thermodynamic properties of volume and total energy cannot be generally used as criteria for amorphization. Instead it was found that, at the completion of amorphization, the magnitude and distribution of the atomic level shear stress was identical to that of the glassy state formed by a quench from the liquid. It is suggested that the atomic level shear stress provides a universal criterion for the attainment of the amorphous state, through glass transition, alloying, and solid state amorphization.

1. Introduction

As applications for metallic glasses have rapidly increased, intensive and systematic studies of amorphization have escalated as well. Beyond the classical means of creating metallic glasses, *i.e.* rapid quenching of alloy melts, electrodeposition, and vapor and sputter deposition, newer solid state amorphization techniques have been developed: mechanical alloying, interdiffusion reactions, and particle irradiation, to name a few. These new developments have led to more fundamental questions directed toward understanding the crystal-to-amorphous (CA) transformation.

In this paper, we will concentrate on amorphization through particle irradiation, specifically via electron bombardment. When an intermetallic compound is bombarded by energetic particles such as electrons, the crystal structure absorbs damage in the form of point defects or point defect complexes. This accumulation of damage can eventually lead to amorphization. The possibility of amorphization depends on the composition and temperature. The criteria and mechanism for amorphization have been the subject of several recent studies [1, 2]. It has been suggested that the CA transformation is akin to melting, and the increase in volume and energy leads to an instability in the crystal which drives amorphization [3]. The purpose of this paper is to show that the atomic level stresses are much better parameters for describing amorphization than volume and energy, and the use of these parameters leads to a much more fundamental understanding of the transition.

Computer simulations of defect-induced amorphization have allowed for more detailed studies of the amorphization process. These simulation techniques allow for the study of the effect of specific defect types, *i.e.* Frenkel pairs or antisite defects, on the propensity for amorphization. In radiation-induced amorphization experiments, it is impossible to separate Frenkel defects and antisite defects experimentally, so it becomes difficult to determine the mechanism of amorphization. Although few pure metals have been amorphized, the first simulations were carried out on point defects in monoatomic systems [4]. Recently, with the development of the embedded atom method and *N*-body potentials, much work has been done on binary compounds, especially those in the Cu–Ti system [2, 5–7]. Although these studies have closely examined the CA transition, none has asked the basic question of how to describe the amorphous solid. Before the transition can be understood, there has to be a greater understanding of the glass.

Several recent studies [8–11] have shown that the atomic level stress tensor provides a good description of the kinetics and structure of liquids and glasses, and has been used to study the transition from liquid to glass. In this study, we use molecular dynamics (MD) to examine the distribution of the atomic level shear stresses to determine the point at which the crystal transforms to a glass. We propose that, for a particular

*Paper presented at the Symposium on Solid State Amorphizing Transformations, TMS Fall Meeting, Cincinnati, OH, October 21–24, 1991.

system, the shear stress distribution, which can be parameterized using the mean shear stress and the fourth-order cumulant, is independent of how the glass was formed. Therefore, these values should be used in determining when the glass is present, and are thus the parameters which indicate the transition from crystal to glass. We chose the Cu–Ti system to study since much simulation work [2, 5, 6] has been previously done, and a large amount of experimental data were at our disposal [12–16]. The results of our study show that the atomic level shear stress distribution can be used as a criterion for the completion of the CA transition, and that the dependence of the volume and total energy on the history of the glass severely restricts their application to the understanding of the transition.

Section 2.1 introduces and defines the atomic stress tensor. This is the important parameter in describing the glass, and is used to characterize the local atomic structure. In Section 2.2, we introduce our interatomic interaction model which is an empirical many-body potential. The application of many-body potentials has grown significantly in recent years as a result of the increase in computing power and their success in describing many materials properties. The interest in these methods [17–20], for the most part, stems from their ability to describe the effect of large changes in atomic coordination, as well as being unconstrained by the Cauchy relations which are the downfall of standard pair potentials. We chose to use N-body potentials of the Finnis–Sinclair type because of the availability of pure metal potentials. In this section we also discuss the simulation procedure and method. In Section 3 we describe results from two types of atomic position analyses. A projection of the atoms in the MD box onto a (001) plane is used to help assess crystallinity.

This analysis is complemented by another investigation using pair distribution functions at different defect concentrations. These methods are used as a check for crystallinity since they are by themselves inadequate in determining when amorphization occurs. Sections 4 and 5 contain the important results of this study. In Section 4, we investigate the premise that the thermodynamic properties of volume and energy can be used as criteria for determining amorphization. We present our data showing that this premise is not valid for this system. We show in Section 5 that the atomic level shear stress provides a reliable parameter for describing amorphization. Our data indicate that the average shear stress and the fourth-order cumulant provide the important criteria for amorphization. We summarize our results in Section 6.

2. Basic building blocks

2.1. Atomic level stresses

Although stress is usually defined in a macroscopic continuum, it is possible to extend the concept to an atomistic level. The stress can be used to characterize the local atomic structure of any system, for example the local structure of liquids, glasses and crystalline defects [10], as long as the stress can be attributed to every individual atom. In this way, the description of local atomic structure is converted from the usual scalar quantity, local density, to a tensorial quantity, the stress tensor [21]. The atomic level stress associated with an atom i is defined such that the total stress is

$$\sigma^{\alpha\beta} = \frac{1}{V}\sum_i \Omega_i \sigma_i^{\alpha\beta} \tag{1}$$

where $\sigma_i^{\alpha\beta}$ is the $\alpha\beta$ cartesian component of the stress tensor associated with atom i, Ω_i is the volume of the Wigner–Seitz (Voronoi) cell of atom i, and V is the total volume of the system [21]. General expressions for the atomic level stresses can be derived using the method of uniform strains, provided that the energy of the system can be written as a sum of the energies associated with individual atoms. When the total potential energy of the system is only a function of the separations between the atoms, which is the case for the many-body potentials used here, the change in energy due to a small applied macroscopic strain $\epsilon_{\alpha\beta}$ is [22]

$$\Delta E = \frac{1}{2}\sum_{\alpha,\beta=1}^{3}\sum_{i,j=1}^{N} f_{ij}^{\alpha} r_{ij}^{\beta} \epsilon_{\alpha\beta} \tag{2}$$

where r_{ij} is the separation of atoms i and j, f_{ij} is the force on atom i due to atom j, and α, β are the cartesian components. In the continuum model, this small change in energy can be written as

$$\Delta E = \sum_{\alpha,\beta=1}^{3} \Omega_i \sigma_i^{\alpha\beta} \epsilon_{\alpha\beta} \tag{3}$$

where $\sigma_i^{\alpha\beta}$ is the microscopic stress associated with atom i. Using these two equations, the atomic level stresses can be written as

$$\sigma_i^{\alpha\beta} = \frac{1}{\Omega}\left(\sum_j f_{ij}^{\alpha} r_{ij}^{\beta} - M_i v_i^{\alpha} v_i^{\beta}\right) \tag{4}$$

where the second term in the parentheses represents the finite temperature correction, and v_i and M_i are the velocity and mass respectively of this atom. It has been shown that the average stress in the MD box is equal to the macroscopic stress [10]. It should be noted that this does not mean that there are stresses present in the system at a macroscopic scale; rather, it is possible for the system to support local stresses as long as the

average over the box goes to zero or the fluctuations in the stresses are dynamic. In crystals static fluctuations may be present only around defects [23].

In liquids and glasses, large fluctuating atomic level stresses exist, and they have been used in elucidating various properties of metallic glasses [8, 11, 24]. The most important characteristics of the atomic level stress tensor can be represented by two rotationally invariant parameters,

$$p = \mathrm{Tr}(\sigma)/3 \tag{5}$$

$$\tau = \left(\frac{1}{6}\right)^{1/2} [(\sigma_1 - \sigma_2)^2 + (\sigma_2 - \sigma_3)^2 + (\sigma_3 - \sigma_1)^2]^{1/2}$$

where σ_1, σ_2 and σ_3 are the principal stresses. The first is the hydrostatic stress which is related to the local volume fluctuations, and the second parameter is the average (von Mises) shear stress which describes the distortion of the atomic environment away from spherical symmetry. Note that the von Mises shear stress is the r.m.s. of the shear components of the stress tensor, so $\langle\tau\rangle \neq \langle\tau\rangle = 0$. From this point, all references to the shear stress will be taken to mean the von Mises shear unless noted otherwise. Since the shear stresses that are being characterized are the square root of the second moment, which is equal to the second-order cumulant since $\langle\tau\rangle = 0$, the fourth-order cumulant $\langle\tau^4\rangle_c$ is used to characterize the shape of the distribution of the atomic shear stresses. The fourth-order cumulant is defined as

$$\langle\tau^4\rangle_c = \langle\tau^4\rangle - 3\langle\tau^2\rangle^2 - 4\langle\tau\rangle\langle\tau^3\rangle + 12\langle\tau\rangle^2\langle\tau^2\rangle - 6\langle\tau\rangle^4 \tag{6}$$

Since $\langle\tau\rangle = 0$, eqn. (6) can be reduced to

$$\langle\tau^4\rangle_c = \langle\tau^4\rangle - 3\langle\tau^2\rangle^2 \tag{7}$$

2.2. The model and methodology

As stated earlier, this study is an examination of a defective Cu–Ti alloy: more specifically, $CuTi_2$ (Fig. 1).

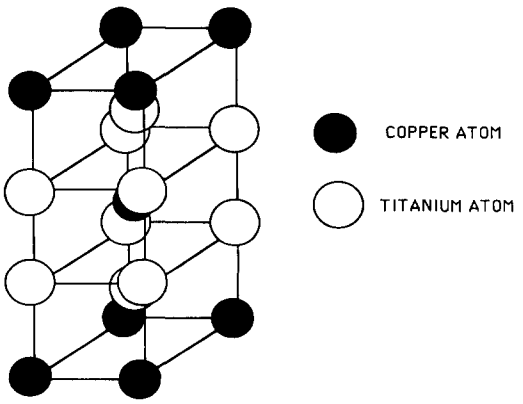

Fig. 1. Crystal structure of $CuTi_2$.

This system is a body-centered tetragonal structure based on $MoSi_2$ with six atoms per unit cell, and the motif consists of linear chains of $CuTi_2$ aligned parallel to the c axis. An MD simulation was carried out using 1152 atoms in an $8\times8\times3$ configuration of $CuTi_2$ unit cells in a constant stress–number–enthalpy MD mode with periodic boundary conditions [25, 26]. This simulation method allows for changes in the shape of the MD box. The atoms in this simulation interact through N-body potentials of the Finnis–Sinclair type [17].

Using the Finnis–Sinclair formalism, the total energy of a system of N atoms can be written as

$$E = \frac{1}{2}\sum_{i\neq j=1}^{N} V_{ij}(R_{ij}) - \sum_{i=1}^{N} \rho_i^{1/2} \tag{8}$$

where V_{ij} is a pair potential which describes the interaction between atoms i and j separated by the distance R_{ij}, and ρ_i, which represents the local electronic density in the volume associated with atom i, is written as $\rho_i = \Sigma_j \Phi_{ij}(R_{ij})$ where Φ_{ij} is also a pair potential. The second term is the many-body part of the energy and its square root functional can be justified in the framework of a second moment approximation to tight-binding theory [27]. Φ_{ij} can be interpreted as the square of the hopping integral and thus can be thought of as an effective coordination [28]. This interpretation is backed by Robertson and Heine's [29] recent results from *ab initio* calculations which have demonstrated that the energy scales as the square root of the coordination.

In expanding these potentials to binary alloys [30], the ij of the pair potentials V and Φ refer to the chemical species of atoms i and j. Therefore, for binary systems there are six potentials: V_{AA}, V_{BB}, V_{AB}, Φ_{AA}, Φ_{BB} and Φ_{AB}. Assuming that V_{AA}, V_{BB}, Φ_{AA} and Φ_{BB} are independent of concentration [31], the same potentials as those calculated for the pure metals are used, and Φ_{AB} is given as the geometrical mean of Φ_{AA} and Φ_{BB} which is consistent with its interpretation in terms of hopping integrals. Thus, only V_{AB} has to be fitted to the alloy properties.

The functional form of V_{AB} is the same as that used for the pure metals [31] for consistency. Thus, cubic splines are used as the form of the potentials,

$$V_{AA}(R_{ij}) = \sum_{k=1}^{6} a_k^{AA} H(r_k^{AA} - R_{ij})(r_k^{AA} - R_{ij})^3$$

$$\Phi_{AA}(R_{ij}) = \sum_{k=1}^{4} A_k^{AA} H(R_k^{AA} - R_{ij})(R_k^{AA} - R_{ij})^3$$

$$V_{AB}(R_{ij}) = \sum_{k=1}^{6} a_k^{AB} H(r_k^{AB} - R_{ij})(r_k^{AB} - R_{ij})^3$$

$$\Phi_{AB}(R_{ij}) = [\Phi_{AA}(R_{ij})\Phi_{BB}(R_{ij})]^{1/2} \tag{9}$$

where r_k and R_k are cut-off distances chosen such that $r_1 > r_2 > \ldots > r_6$ and $R_1 > R_2 > R_3 > R_4$, and $H(x)$ is the

Heaviside step function. The coefficients a_k^{AA} and A_k^{AA} are fitted to the equilibrium properties of the pure metal: lattice parameters, cohesive energy, elastic constants, the lower bound of the unrelaxed vacancy formation energy, and the stacking fault energy. The coefficients a_k^{AB} are fitted to the properties of the alloy: heat of formation, elastic constants (when available), and stability of the equilibrium alloy crystal structure.

For this study, the published potentials for Cu [32] and Ti [33] were not sufficient. A new Ti potential was derived to eliminate a negative "bump" in Φ_{TiTi} which caused Φ_{CuTi} to become imaginary at certain separations, and a stronger short-range repulsion was added to the Cu potential to stabilize the crystal structure. In determining the alloy potential, a LMTO calculation was performed to obtain an approximate bulk modulus to help in the fitting. Table 1 summarizes the coefficients used to describe the potentials. These potentials have been used successfully in a study of vitrification [34], and further details and the development of these potentials can be found elsewhere [35].

The simulation was carried out using an integration time step of 1.0×10^{-15} s, and the temperature was maintained at 25 K by continuously rescaling the kinetic energy. The simulation procedure was conducted as follows. The perfect lattice was equilibrated at 25 K for 50 000 time steps (TSs), and then Frenkel pair defects were created every 100 TSs by randomly choosing an atom, removing it from the crystal, leaving behind a vacancy, and then reinserting the atom at some random interstitial site (at least 1 Å away from any other atom). The atomic configurations were saved at regular intervals for later analysis. Three separate defect runs were carried out using this procedure. Two quench runs were also performed. The first was a single time step quench from an equilibrated liquid at 2500 K to a glass at 25 K followed by a 10^4 TS relaxation. The second quench was slower than the fast quench, and proceeded in steps of 200 K with a 10^5 TS hold at each step for equilibration. For all runs, including the quenches, the configurations were analyzed by examining the atomic projections, pair distribution function (PDF), volume, total energy, average shear stress and fourth-order cumulant. The quench runs were used as the glass standards for our investigations.

TABLE 1. Parameters of N-body potentials for Cu, Ti, and V_{AB}

	Cu	Ti	Cu–Ti
a_1	61.73525861	−57.099097	0.07354373
a_2	−108.1846788	80.735598	−0.65429048
a_3	57.00053948	−21.761468	2.25129739
a_4	−12.88796578	−10.396479	0.0
a_5	39.16381901	74.515028	0.0
a_6	200.0	35.921024	0.0
A_1	10.03718305	39.795927	
A_2	17.06363299	−40.061305	
r_1	1.225	1.22	4.95
r_2	1.202	1.20	3.90
r_3	1.154	1.12	3.30
r_4	1.05	0.95	2.00
r_5	0.866	0.80	1.50
r_6	0.740	0.707107	1.0
R_1	1.225	1.22	
R_2	0.990	1.05	
a (Å)	3.615	4.173061	2.9438, 10.7861

We use normalized coefficients for the pure metals and absolute units of ångströms and electronvolts per cubic ångström for r^{AB} and a^{AB} respectively.

3. Atomic position analysis

In order to gain a greater insight into the effect the introduction of Frenkel defects has on the crystalline order in the alloy studied, a visual inspection of the atomic positions and the calculation of the PDF were conducted at various defect concentrations. Although these methods will not on their own give reliable evidence of amorphization, these methods are sensitive to the presence of crystallinity and can be used to assess the level of amorphization. The results in this section will be broken into two parts, and each will be preceded by a brief explanation of the technique used and the applicability of the results toward an overall understanding of defect-induced amorphization.

It was decided that a reasonable means to inspect visually and to determine qualitatively the damage to the model crystal during the introduction of defects was by means of a projection of the atomic positions onto the (001) plane. This allows for a two-dimensional viewing of the MD box. If the crystalline lattice is present then the underlying symmetry will be seen as fringing in well-determined directions in the projection. Of course, this method cannot be used as independent evidence confirming the transition to the amorphous state, but it can be used to determine the minimum defect concentration where the system may be amorphous.

Figure 2 shows plots of the projections of all the atoms in the MD box onto the (001) plane at various defect concentrations. For no defects, Fig. 2(a), note that the atomic columns are well aligned. Since the simulation temperature is only 25 K, thermal vibrations play almost no part in the initial atomic positions. The most dominant fringing patterns, at this orientation, are the diagonal ⟨11⟩-type fringes. There are visible fringes in the ⟨10⟩ and ⟨01⟩ directions as well. At a

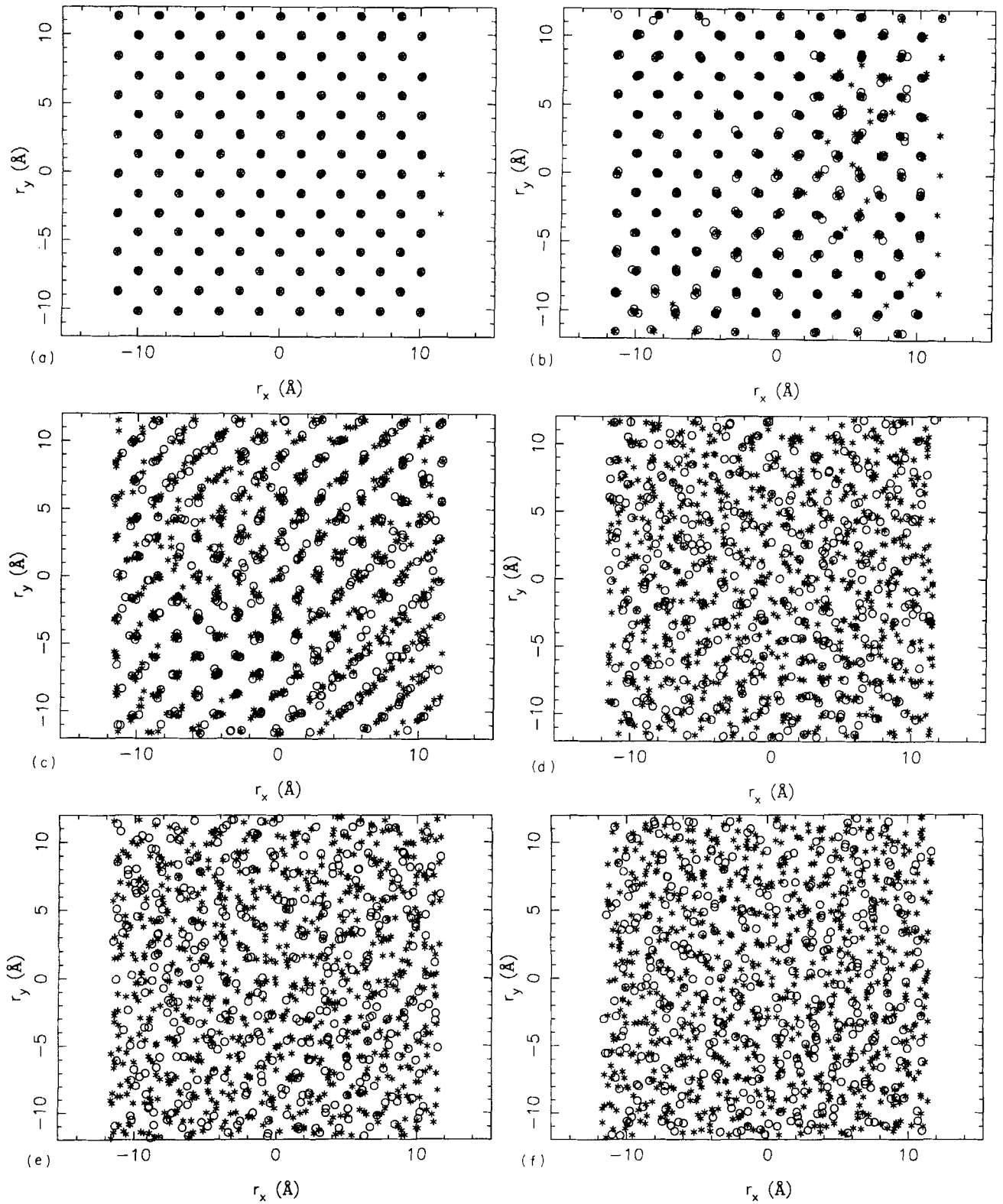

Fig. 2. Projection of all atoms in the MD box onto the (001) plane for different defect concentrations: (a) no defects; (b) 0.0174 DPA; (c) 0.174 DPA; (d) 0.330 DPA; (e) 0.417 DPA; (f) 0.521 DPA.

defect concentration of 0.0174 defects per atom (DPA), local disruptions of the lattice configuration can be seen, as well as the presence of interstitial atoms (Fig. 2(b)). Large areas of crystal are still present, and the atomic columns, for the most part, are still intact. The fringes in all directions are still visible, leading one to

assume that the system is still dominated by the crystal. As the defect concentration was increased by an order of magnitude to 0.174 DPA (see Fig. 2(c)), a large area of disrupted crystal on the right edge is seen, although large areas of crystalline order are still present. The damage seems to be particularly severe in the lower right-hand corner and continues, as a result of the periodic boundary conditions, in the upper right-hand corner. Although the atomic columns seem to be disrupted in this region, fringing in all directions is still visible. Up to 0.2 DPA, the fringes associated with the crystal are the dominant features, and indicate that the properties of the system should still be dominated by the crystalline order.

Increasing the defect concentration to nearly one-third (0.330 DPA) leads to what looks like a completely disordered system with widely scattered atomic positions (Fig. 2(d)). The atomic columns aligned with the c axis, which corresponds to the orientation of the crystal motif, have been nearly eliminated. Examination of the fringes within the plane of the paper, however, shows that the ⟨10⟩ and ⟨01⟩ fringes are still present, but nearly lost. The ⟨11⟩ fringes are still relatively strong, indicating the presence of some ordering. One should note that there are no perceptible regions where all fringing has been lost. Regions where ordering in some directions have been lost maintain ordering in the other directions. This indicates that there is still an underlying crystalline symmetry. Figures 2(e) and 2(f) (0.417 DPA and 0.521 DPA respectively) show the concentration where crystallinity is seemingly lost. In Fig. 2(e), ⟨11⟩-type lattice fringes are barely perceptible, and one might argue the presence of a few ⟨10⟩ fringes. This indicates that it may not be reasonable to consider the system amorphous because of the presence of the crystal-like pattern, even though it seems to be a minority phase. For the 0.521 DPA case (Fig. 2(f)), there is a complete loss of fringing, as far as can be determined by eye. From these results one could assume that amorphization did not occur at defect concentrations below 0.417 DPA.

To augment the visual inspection of the atom projections, a series of PDFs were calculated to verify the presence of crystal. The PDF analysis produces more quantitative evidence for residual crystallinity in defective systems. This method, like the projection method, is sensitive to the presence of crystal through the presence of peaks which do not correspond to pair correlations present in the glass. The main advantage of calculating PDFs is that they represent experimentally verifiable results and can be compared with experimentally determined PDFs. This method, however, is not reliable in determining when a system is completely amorphous. It is difficult to determine the exact circumstances where all crystalline peaks disappear, so it remains a good indicator for determining whether a system is not amorphous rather than whether it is. One should also realize that the PDF is a spherical average so all orientational information is lost.

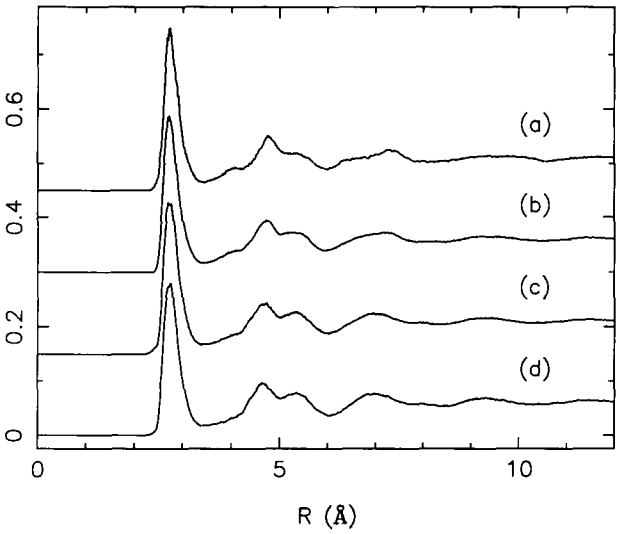

Fig. 3. Simulated atomic PDF of $CuTi_2$ for different defect concentrations: curve a, 0.330 DPA; curve b, 0.417 DPA; curve c, 0.521 DPA; curve d, the glass.

The PDFs in this study are calculated using the following formula:

$$\mathrm{PDF} = \rho(r) = n(r)/4\pi r^2\,\delta r \tag{10}$$

where the PDF $\rho(r)$ is defined here as the ratio of the number $n(r)$ of atom pair separations of distance r to the volume of the shell with radius r and thickness δr. Curves a–c in Fig. 3 correspond to the defect concentrations of the projections of Figs. 2(d)–2(f) respectively and are used to verify the presence of crystal. Figure 3, curve d, is the PDF calculated from the fast quench run, and is used as the standard for the glass. Figure 3, curve a, 0.330 DPA, has features not present in Fig. 3, curve d, the glass. The small peak at 4 Å and the split third nearest neighbor (3NN) (6.0–8.0 Å) peak are indicative of partially crystalline $CuTi_2$. In Fig. 3, curve b, the 0.417 DPA system still shows some signs of crystallinity as well. The small peak at 4 Å is barely visible and the multiple peak at the 3NN position is still present. In Fig. 3, curve c, the PDF looks very similar to that of a glass (Fig. 3, curve d). The 3NN and 4NN peaks are definitely single peaked, and there is no sign of the small peak at 4 Å. These results confirm our analysis of the atom projections. This evidence corroborates our interpretation that the visible fringes in the atom projections correspond to the presence of crystallinity. From the PDF data, it can be determined that amorphization did not occur at defect concentrations below 0.417 DPA as in the case with the atom projections.

4. Volume and total energy *vs* defects per atom

Figure 4 is a plot of the dependence of the atomic volume on the defect concentration. The figure represents three different runs as described earlier. For less than 0.065 DPA, the volume increases linearly with increasing defect concentration. This linear increase represents the elastic expansion of the lattice due to the insertion of the interstitials. When the defect content becomes high enough, recombination of interstitials and vacancies begins to occur, and thus the volume increases less rapidly. The volume eventually saturates when the defect concentration reaches 0.20 DPA with a volume near 16.680 $Å^3$ $atom^{-1}$. This saturation indicates that the recombination occurs within the time scale of defect production. Although the atomic volume has saturated, except for a small peak in run 3, the system is still mostly crystalline at 0.20 DPA according to the atom projection and PDF data of Section 3, which reveals partial crystallinity at defect concentrations below 0.417 DPA. This plateau represents an increase of 5.50% over the equilibrium volume at 25 K, which is a remarkably large amount considering that the volume of the glass usually exceeds that of the crystal by roughly 1.0%–3.0%. The two horizontal lines marked a and b represent the volume of two glasses formed at different cooling rates, as described in Section 2. The data cross the slow quench line b around 0.022 DPA and the fast quench line a near 0.09 DPA, which is well within the crystalline region as determined from the data of Section 3. The filled circles in Fig. 4 represent the volume after relaxation over 10^5 TSs. These runs were conducted at defect concentrations of 0.174, 0.260, 0.347, 0.451, 0.521, and 0.694 DPA. In all cases, there were significant drops in volume, after relaxation, ranging from 1.5% to 4.0%. Using the PDFs (Fig. 3), it was judged that the two samples at 0.521 and 0.694 DPA were amorphous, and the other four were still crystalline. The volumes reported are stable to within 0.7%, which correspond to errors of less than 0.115 $Å^3$ $atom^{-1}$.

As noted earlier, it has been proposed that, if the volume expansion induced by defect production causes the volume of the defective crystal to exceed the volume of the glass, then amorphization will occur as a result of mechanical instability [3]. The results above show that this hypothesis is not valid for $CuTi_2$. Moreover, the volume of the glass is very dependent on the quench rate as seen in Fig. 4. In fact, the volume of the slow-quenched glass is closer to the volume of the non-defective crystal than to that of the defective crystal or even the fast-quenched glass. The large drops in atomic volume during relaxation indicate that the atomic volume is also very dependent on the relaxation of the defective system. The value of the atomic volume is not unique to the glassy state, since the slow-quenched and 0.694 DPA relaxed glasses have the same volume as the partially crystalline system, unrelaxed, at 0.022 DPA. Thus, the atomic volume is not a useful parameter for amorphization.

Figure 5, total energy per atom *vs.* defect concentration, shows similar properties to Fig. 4. In this case, the total energy reaches a plateau near a value of −4.3 eV $atom^{-1}$ at 0.310 DPA. The atomic structure at this defect concentration can be characterized by Fig. 2(d), which still has strong ⟨11⟩ fringes, and the partially crystalline PDF of Fig. 3, curve a. Again the horizontal lines marked a and b represent the fast- and slow-quenched glass respectively. In this case the data cross the lines at higher defect concentrations. The slow quench is crossed at 0.095 DPA and the fast quench is crossed at 0.150 DPA. For both cases the system is still crystalline at the cross over points. As in the case

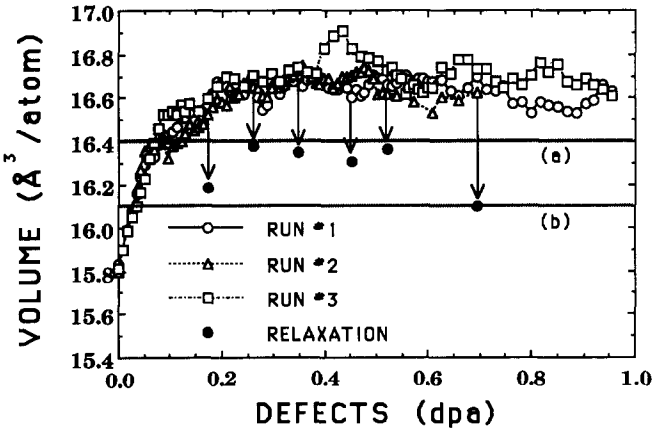

Fig. 4. Dependence of volume per atom on defect concentration for all three runs. The lines represent the volumes of the fast- (line a) and slow- (line b) quenched glasses, and the arrows show the drop in volume after relaxation.

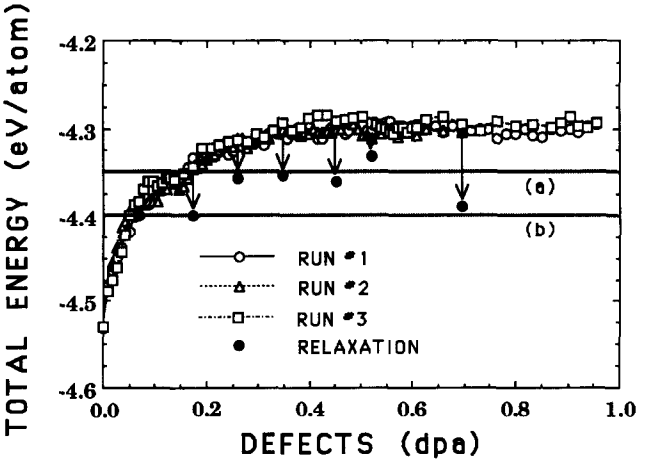

Fig. 5. Dependence of total energy per atom on the defect concentration for all runs. The lines represent the values of the fast- (line a) and slow- (line b) quenched glasses, and the arrows show the drop in energy after relaxation.

of atomic volume *vs.* DPA, the total energy per atom is very dependent on the quench rate. There is a huge difference between the energies of the fast-quenched glass and the plateau, close to 0.5 eV atom^{-1}, and the difference between the fast- and slow-quenched glasses is large as well. Thus the energy cannot be used as the parameter to judge amorphization. During relaxation, the energy exhibits significant drops in energy, as much as 2.0%. As in the case of the atomic volume, these data suggest that there is no unique energy which describes the glassy state. The statistical errors in total energy are within $3/N$ which is 0.26% and corresponds to errors of less than 0.011 eV atom^{-1}.

The defect concentration dependences of the atomic volume and the total energy per atom show that the thermodynamic properties are not useful as criteria for amorphization. In both cases the properties surpass the values of the quenched glass and reach a plateau well before complete amorphization. Relaxation of the glass results in decreases in both the atomic volume and the total energy to levels equal to that of the unrelaxed partially crystalline state. This indicates that knowledge of the relaxation history of the system is necessary, and that no value of these properties is unique to the glass. Thus it is necessary to find a more reliable criterion for amorphization. We found that the atomic level stresses provide a reliable measure of amorphization and are thus a viable criterion.

5. Atomic level shear stress analysis

Figure 6 is the distribution of the shear stresses in the $CuTi_2$ alloy in three different states. The horizontal axis, in all three cases, is the value of the von Mises shear stress. The first, Fig. 6(a), is the distribution in the non-defective crystal at 25 K. It should be noted that the distribution is bimodal, with each value sharply defined and representing one of the two atom types present in the system.

Figure 6(b) shows the distribution in a defective crystal at only 0.01 DPA. The sharp peaks from the non-defective case have been reduced by a factor of 7 and largely broadened. This indicates how sensitive the shear distribution is to changes in the structure of the system. The distribution in a quenched glass is shown in Fig. 6(c). This distribution takes the form of a five-dimensional gaussian which is expected for metallic glasses [11]. The average value of the atomic shear stress distribution is simply the mean and, since τ is defined as the r.m.s. of the independent shear stress, the fourth-order cumulant $\langle \tau^4 \rangle_c$ would then be an expression of the shape of the distribution. By looking at these two values, the transition from the partially

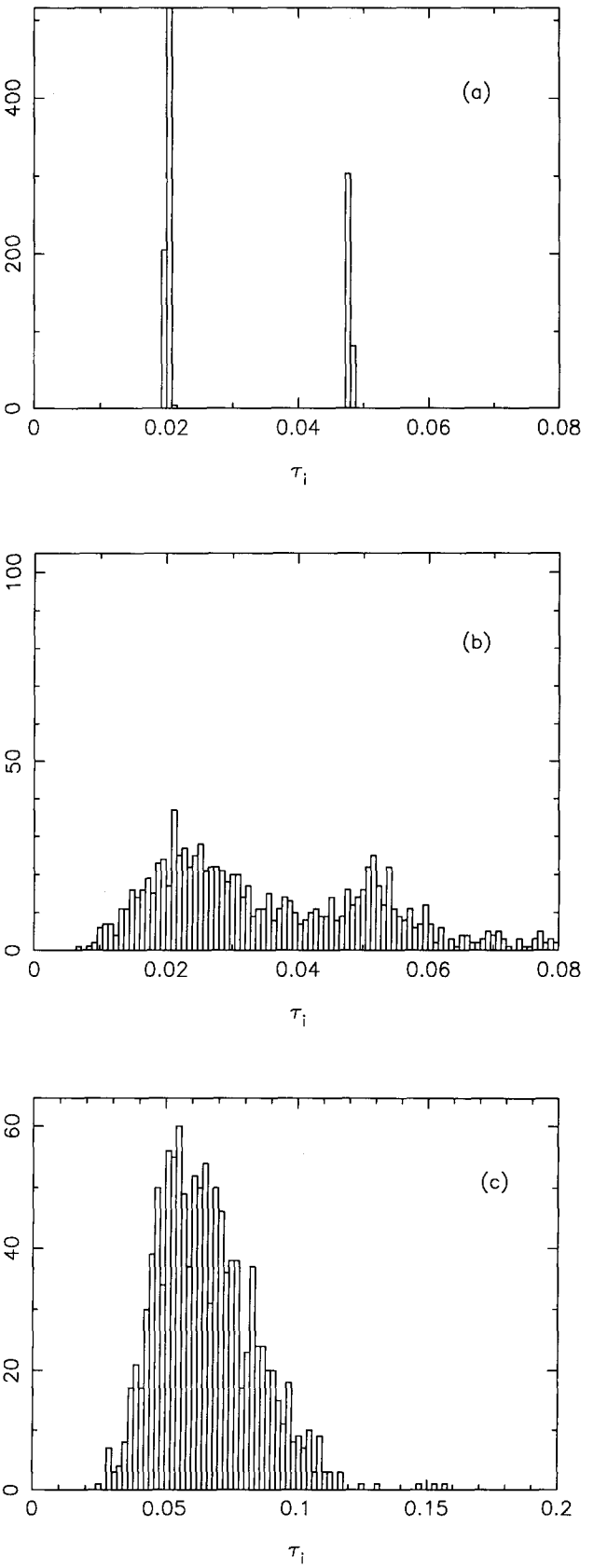

Fig. 6. Histograms showing the distribution of the atomic level shear stress in (a) the perfect crystal, (b) a defective crystal at 0.01 DPA, and (c) the glass.

crystalline state to the amorphous state should be well defined if the shear stress distribution is universal for all glasses with the same composition.

Figure 7 is a plot of the dependence of the average shear stress on the defect concentration. For the purpose of normalization, the shear stress is divided by twice the shear modulus G (0.4973 eV Å^{-3}), averaged over the last 100 steps, to obtain the average local shear strain. The curves reach a plateau around 0.50 DPA at a shear strain value of 0.065 which is an increase of 124% over the crystal value, which mirrors our earlier stipulation of the sensitivity of τ to changes in the atomic environment. It should be noted that the atom projection inspection (Fig. 2) and the PDFs (Fig. 3) indicate that the CA transition takes place around these defect concentrations. Also, experiments using 2 MeV H^+ at 98 K on $CuTi_2$ suggest that complete amorphization occurs between 0.43 and 0.65 DPA [12]. The saturation value of the shear strain, 0.065, is very close to the values from the quench runs, which are 0.0638 for line a and 0.0651 for line b. The changes in these values due to relaxation, at 0.521 and 0.694 DPA, are so small that they do not show at this scale. For defect concentrations under 0.451 DPA, there are significant drops in the average shear strain away from the glass levels. Thus $\langle\tau\rangle$ seems to be independent of relaxation in the glass, and dependent on relaxation in the crystal. This is different from the large changes seen in the atomic volume and total energy. This indicates that the average shear stress is nearly independent of the processing history and is likely to be an intrinsic property of the glass.

In Fig. 8, the fourth-order cumulant, which is divided by $(\langle\tau^2\rangle_f)^2$ (which is the same as $(\langle\tau^2\rangle_f)^2$) averaged over the last 100 steps for the purpose of normalization, is plotted as a function of defect concentration. The plot shows that $\langle\tau^4\rangle_c/\langle\tau^2\rangle^2$ decreases linearly with

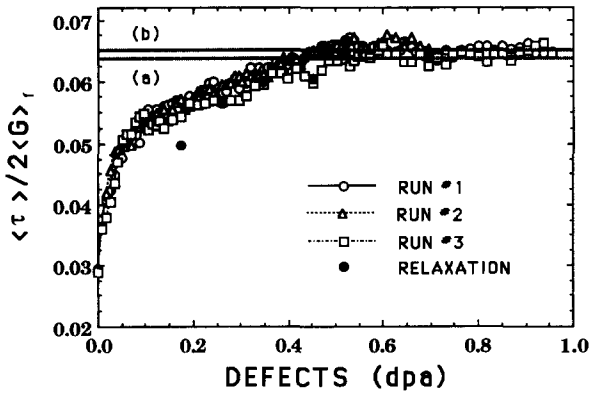

Fig. 7. Variation in the average shear stress $\langle\tau\rangle$, normalized by twice the average shear modulus $\langle G\rangle_f$, with the defect concentration. Lines a and b represent the values of the fast- and slow-quenched glasses respectively.

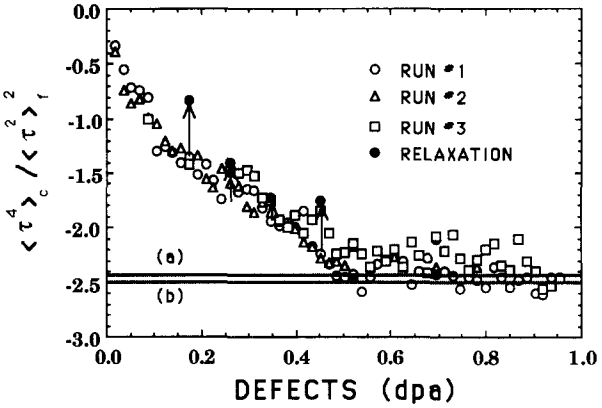

Fig. 8. Variation in the normalized fourth-order cumulant, $\langle\tau^4\rangle_c/(\langle\tau^2\rangle_f)^2$ with the defect concentration. Lines a and b represent the values of the fast- and slow-quenched glasses respectively.

increasing defect concentration up to a concentration of about 0.50 DPA, where the shape of the shear stress distribution becomes independent of further damage. This saturation is also an indication of the CA transition. The value of $\langle\tau^4\rangle_c/(\langle\tau^2\rangle_f)^2$ agrees within the noise with those for the quenched glasses as shown in Fig. 8. The value of $\langle\tau^4\rangle_c/\langle\tau^2\rangle^2 = \langle\tau^4\rangle/\langle\tau^2\rangle^2 - 3$ can be approximated if the distribution of τ is assumed to take the form of a five-dimensional gaussian [8, 11] and that the independent shear stress components are approximately equal. The calculated normalized fourth-order cumulant is -2.52. Examination of Fig. 8 shows that the saturation value is close to this approximation. As in the case of $\langle\tau\rangle$, the fourth-order cumulant in the glass exhibits virtually no change during relaxation, while in the partially crystalline system there is a dependence on relaxation. This indicates that this quantity is also a property of the glass which is independent of processing.

Thus both the average shear stress and the fourth-order cumulant become independent of the defect concentration beyond about 0.5 DPA. This indicates that the magnitude and distribution of the atomic level shear stresses have reached the point of saturation there, and any additional defects become immediately relaxed. Such a state must be the glassy state, since a vacancy and an interstitial defect are known to be unstable in a metallic glass [36], and indeed the PDF indicates a loss of crystallinity.

6. Conclusion

Several recent computer simulation results [1, 2] on defect-induced amorphization have indicated that the pertinent parameters in studying the CA transformation are the volume and total energy as functions of the

defect concentration. Through arguments that the CA transformation is similar to melting, the volume and total energy are signs of mechanical instability within the crystal and should lead to the collapse of the crystalline lattice into a glassy state. This paper has shown that this is not the case. At defect concentrations where both the atomic volume and the total energy have saturated, the atom projections and PDFs clearly show signs of crystallinity, indicating that the crystal is still stable. The thermodynamic properties do not give a unique value for the glass state; rather, they change as the system relaxes to the local minimum. The dependence of the thermodynamic properties on how the glass is formed and how it is relaxed indicates a dependence on the history of the glass, and thus they cannot be used generally to describe amorphization. On the contrary, the average atomic shear strain $\langle\tau\rangle/2G_f$ and the fourth-order cumulant $\langle\tau^4\rangle_c/(\langle\tau^2\rangle_t)^2$ in the glass have been shown to be independent of the history of the glass. Both parameters reached saturation at a value equal to those of two glasses quenched at different rates, and neither changed as the glass was relaxed, while changes are seen after relaxation at defect concentrations below the critical value. Also, the saturation value of the fourth-order cumulant agreed fairly well with an analytic approximation. The concentration where $\langle\tau\rangle/2G_f$ and $\langle\tau^4\rangle_c/(\langle\tau^2\rangle_t)^2$ saturate, 0.50 DPA, corresponds to the concentration where crystalline order disappears in both the atom projection and the PDFs.

The present work has shown that the atomic level shear stresses are effective parameters to describe amorphization. In particular, the radiation damage threshold for complete amorphization can be determined from the magnitude and distribution of the shear stresses. The value of the average shear strain and the distribution of the shear stress were found to be unique to the glass, and can be used to differentiate between the glass and the crystal. In addition, the atomic level stresses have been successfully used in predicting the composition limit of metallic alloys for glass formation by quenching [37] as well as the glass transition temperature [8, 11]. Also, Visscher and Logan [9] found persistent fluctuations of some non-zero k components of the stress near T_g in their simulations of the glass transition. This suggests a universality of the stress criterion in amorphization phenomena in general. The glassy state appears to be characterized by a unique distribution of the local shear stresses, with its average magnitude being dependent only on composition [11]. Excess stresses beyond this state will lead to liquid-like behavior, and at low temperatures they will relax away. On the contrary, stresses cannot be reduced below this state without resulting in partial crystallization. Thus the local stress is an excellent measure of amorphousness and can be used to predict the conditions necessary for amorphization.

Acknowledgment

This work was supported by the National Science Foundation through Grant DMR88-19885.

References

1 P. R. Okamoto and M. Meshii, in H. Wierdersich and M. Meshii (eds.), *Science of Advanced Materials,* ASM International, Metals Park, OH, 1990, p. 33.
2 M. J. Sabochick and N. Q. Lam, *Phys. Rev. B, 43* (7) (1991) 5243.
3 D. Wolf, P. R. Okamoto, S. Yip, J. F. Lutsko and M. Kluge, *J. Mater. Res., 5* (1990) 286.
4 H. Hsieh and S. Yip, *Phys. Rev. Lett., 59* (1987) 2760.
5 M. J. Sabochick and N. Q. Lam, *Scr. Metall., 24* (1990) 565.
6 J. R. Shoemaker, R. T. Lutton, D. Wesley, W. R. Wharton, M. L. Oehrli, M. S. Herte, M. J. Sabochick and N. Q. Lam, *J. Mater. Res., 6*(3) (1991) 473.
7 D. T. Kulp, T. Egami, D. E. Luzzi and V. Vitek, *J. Non-Cryst. Sol.,* in press.
8 S.-P. Chen, T. Egami and V. Vitek, *Phys. Rev. B, 37*(5) (1988) 2440.
9 P. B. Visscher and W. T. Logan, *Phys. Rev. B, 42* (1990) 4779.
10 T. Egami, K. Maeda and V. Vitek, *Philos. Mag. A, 41*(6) (1980) 883.
11 T. Egami and D. Srolovitz, *J. Phys. F, 12* (1982) 2141.
12 J. Chang, M. Yuan, C. N. J. Wagner and A. J. Ardell, *J. Mater. Res., 4* (1989) 565.
13 D. E. Luzzi and M. Meshii, *J. Mater. Res., 1*(5) (1986) 617.
14 D. E. Luzzi and M. Meshii, *J. Less-Common Met., 140* (1988) 193.
15 D. E. Luzzi, H. Mori, H. Fujita and M. Meshii, *Acta Metall., 34*(4) (1986) 629.
16 M. H. Mueller and H. W. Knott, *Trans. Met. Soc., 227* (1963) 6474.
17 M. W. Finnis and J. E. Sinclair, *Philos. Mag. A, 50*(1) (1984) 45.
18 M. S. Daw and M. i. Baskes, *Phys. Rev. B, 29*(12) (1984) 6443.
19 F. Ercolessi, E. Tossati and M. Parrinello, *Philos. Mag. A, 58* (1988) 213.
20 J. K. Norskov and N. D. Lang, *Phys. Rev. B, 21* (1981) 2131.
21 V. Vitek and T. Egami, *Phys. Status Solid B, 144* (1987) 145.
22 M. Born and K. Huang, *Dynamical Theory of Crystal Lattices,* Clarendon, Oxford, 1954, Chap. 1, p. 1.
23 Z. S. Basinski, M. S. Duesberry and R. Taylor, *Can. J. Phys., 49* (1971) 2160.
24 D. Srolovitz, V. Vitek and T. Egami, *Acta Metall., 31* (1983) 335.
25 H. C. Anderson, *J. Chem. Phys., 72*(4) (1980) 2384.
26 M. Parrinello and A. Rahman, *J. Appl. Phys., 52*(12) (1981) 7182.
27 G. J. Ackland, M. W. Finnis and V. Vitek, *J. Phys. F, 18* (1988) L153.

28 G. J. Ackland, *Philos. Mag. A., 66* (1992) 917.
29 I. Robertson and V. Heine, to be published.
30 V. Vitek, G. J. Ackland and J. Cserti, *Mater. Res. Soc. Symp. Proc., 186* (1990) 237.
31 G. J. Ackland and V. Vitek, in V. Vitek and D. Srolovitz (eds.), *Atomistic Simulations of Materials: Beyond Pair Potentials,* Plenum, New York, 1989.
32 G. J. Ackland, G. Tichy, V. Vitek and M. W. Finnis, *Philos. Mag. A, 56*(6) (1987) 735.
33 M. Igarashi, M. Khantha and V. Vitek, in V. Vitek and D. Srolovitz (eds.), *Atomistic Simulations of Materials: Beyond Pair Potentials,* Plenum, New York, 1989, p. 203.
34 D. T. Kulp, T. Egami and V. Vitek, to be published.
35 D. T. Kulp, G. J. Ackland, M. Ŝob, V. Vitek and T. Egami, Modelling and simulation, *Mater. Sci. Eng.,* in press.
36 C. H. Bennett, P. Chaudhari, P. Morruzi and P. J. Steinhardt, *Philos. Mag. A, 40* (1979) 485.
37 T. Egami and Y. Waseda, *J. Non-Cryst. Solids, 64* (1984) 113.